ACS OMEGA

http://pubs.acs.org/journal/acsodf

Article

Gas-Sensing Properties of Cu_2S−$MoSe_2$ Nanosheets to NO_2 and NH_3 Gases

Yingang Gui,* Shengyan Zhu, and Xianping Chen

Cite This: *ACS Omega* 2021, 6, 16517−16523

Read Online

ACCESS | Metrics & More | Article Recommendations

ABSTRACT: Cu_2S−$MoSe_2$ was selected as a gas-sensing material to detect NO_2 and NH_3. Based on density functional theory calculations, the adsorption structures, density of states, molecular orbit, and recovery time were studied to analyze the gas-sensing mechanism of Cu_2S−$MoSe_2$ to gases. Calculation results show that Cu_2S clusters receive a stable doping structure on the $MoSe_2$ surface. Compared with intrinsic $MoSe_2$, Cu_2S−$MoSe_2$ shows more excellent adsorption performance to NO_2 and NH_3 due to the active feature of the Cu_2S dopant. After NO_2 and NH_3 adsorption, the energy gap decreases, indicating an improvement of the conductivity, which is greatly significant for gas sensing. For double NH_3 adsorption, the conductivity of the entire system increases more than that of a double NO_2 adsorption system, signifying the sensitivity of Cu_2S−$MoSe_2$ is greater for NH_3 than NO_2. The results of theoretical recovery time show that Cu_2S−$MoSe_2$ is sensitive for NH_3 detection at room temperature (298 K) and NO_2 detection at high temperature (400 K).

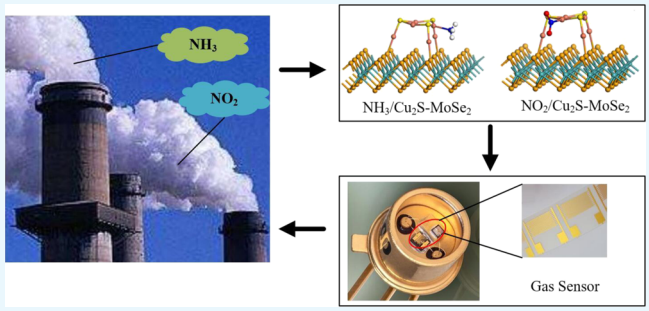

1. INTRODUCTION

With the rapid development of industry and agriculture, more and more toxic gases are being produced and discharged into the atmosphere, which brings a serious threat to human health.[1−4] Among the toxic gases, NO_2 and NH_3 are two important gases due to their high concentration. Therefore, it is very important to monitor and control these toxic gases. Metal oxide semiconductor sensors have been found to be highly sensitive to toxic gases.[5] However, most of them require high operating temperatures, which leads to a high power consumption.[6,7] In recent years, how to develop room-temperature, high-sensitivity, and cheap nanomaterial sensors to accurately and effectively monitor toxic gas molecules has attracted extensive attention of researchers.[8−10]

As a new type of two-dimensional (2D) layered nanomaterial, $MoSe_2$ has a larger surface/volume ratio, which exhibits excellent properties for the adsorption and desorption of the target gases.[6,11] Therefore, it is possible to construct a high-sensitivity room-temperature gas sensor through the change of conductivity caused by gas adsorption.[12,13] In this regard, Late reported an effective single-layer $MoSe_2$ film sensor for NH_3 gas detection at room temperature.[11,14] Chen synthesized a $MoSe_2$ nanosheet as a high-performance room-temperature NO_2 gas sensor using the liquid-phase exfoliation method.[8] However, intrinsic $MoSe_2$ still shows some disadvantages, such as slow charge transfer and low conductivity, which limit its gas-sensing performance.[15]

Studies show that noble metal doping can effectively improve the adsorption performance of $MoSe_2$,[16−18] but the scarcity and high cost of noble metals limit its wide use. As a stable semiconductor, Cu_2S has good conductivity and is widely found in natural ores. Recently, Hassan et al. made Cu_2S grow vertically on $MoSe_2$ and produced a Cu_2S−$MoSe_2$ composite material,[19] which verifies the feasibility of modifying $MoSe_2$ by the Cu_2S dopant. However, so far there are still no reports on the gas-sensing application of Cu_2S−$MoSe_2$ for NO_2 and NH_3 detection.

Herein, we calculated the stable structure of the Cu_2S cluster modified on $MoSe_2$, and studied its adsorption performance for NH_3 and NO_2 based on first-principles calculations. According to the analysis of the adsorption structures, density of states (DOS), partial density of states (PDOS), molecular orbit, and recovery time, it is found that the Cu_2S−$MoSe_2$ shows better adsorption performance and sensing ability for NH_3 and NO_2 than intrinsic $MoSe_2$, suggesting that Cu_2S−$MoSe_2$ can be used as a promising high-sensitivity NH_3/NO_2

Received: March 30, 2021
Accepted: June 8, 2021
Published: June 17, 2021

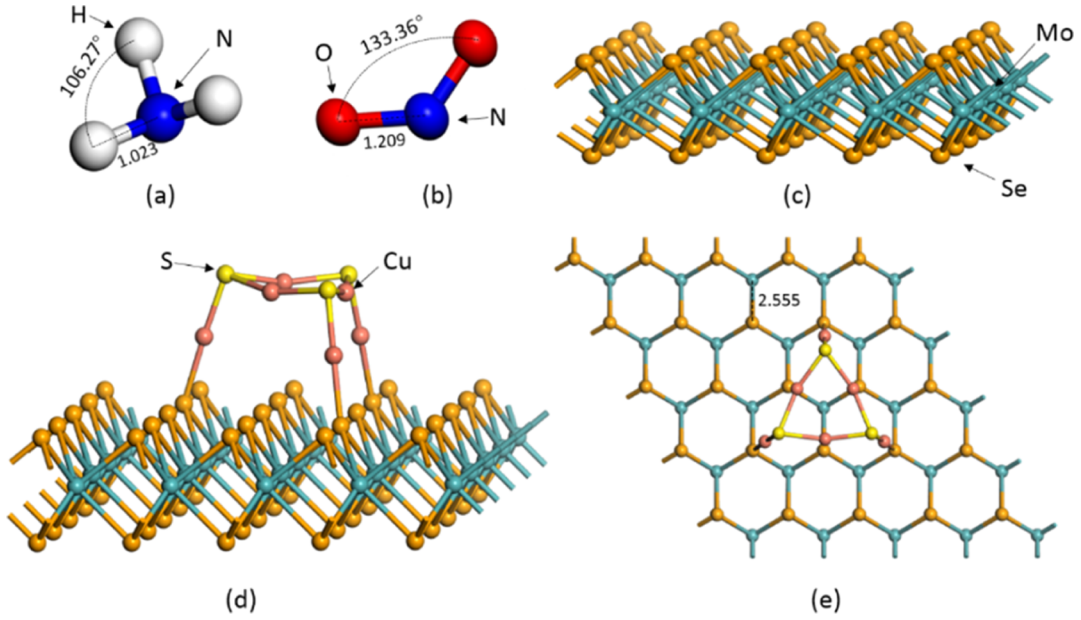

Figure 1. (a) NH_3, (b) NO_2, (c) $MoSe_2$, and (d,e) Cu_2S−$MoSe_2$ in top and side views. The distance is in Å.

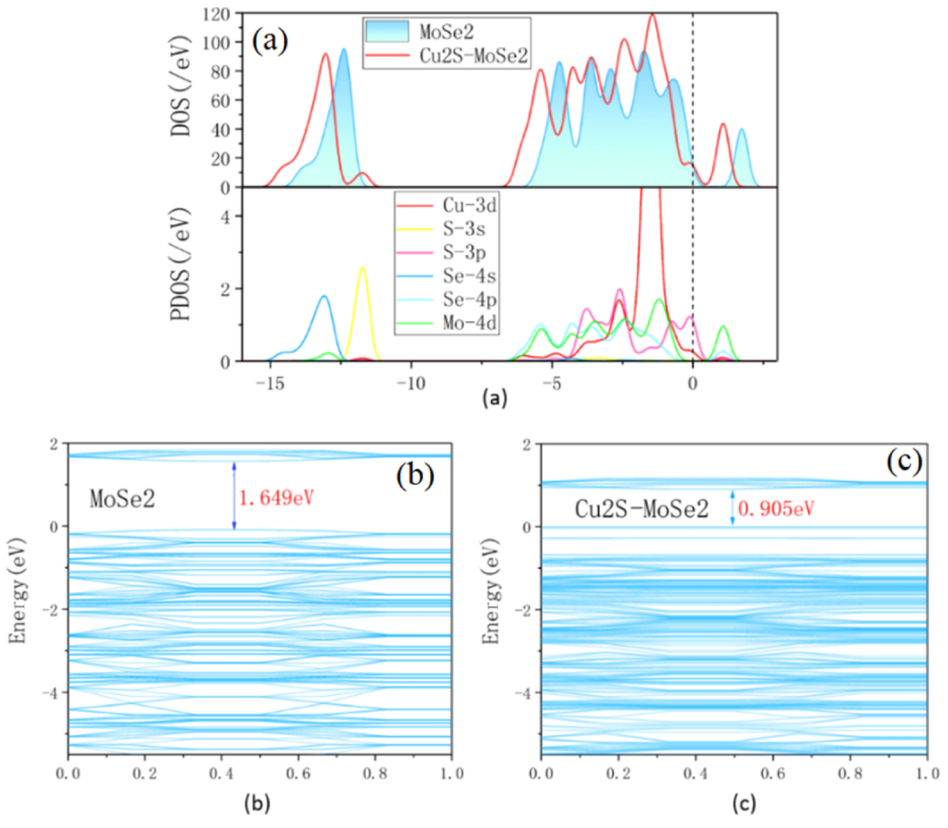

Figure 2. (a) DOS and PDOS of $MoSe_2$ and Cu_2S−$MoSe_2$ and the band structure of (b) $MoSe_2$ and (c) Cu_2S−$MoSe_2$.

gas-sensing material. This study provides a theoretical basis for the experimental development of a Cu_2S−$MoSe_2$ sensor.

2. COMPUTATIONAL METHOD

In this work, all calculations were carried out based on density functional theory (DFT) in Dmol3 of Materials Studio.[20,21] A single-layer $MoSe_2$ supercell was built, including 25 Mo atoms and 50 Se atoms, with a periodic boundary condition of 16.635 Å × 16.635 Å × 28.345 Å. In order to calculate the geometry optimization and energy, a generalized gradient approximation with the Perdew−Burke−Ernzerhof (GGA-PBE) function was chosen.[22,23] The maximum stress, max displacement, and energy tolerance accuracy were, respectively, set to 2×10^{-3} Ha/Å, 5×10^{-3} Å, and 1×10^{-5} Ha.[24] The Brillouin zone *k*-point sampling was performed using a 7 × 7 × 1 Monkhorst−Pack mesh, which presents good approximation for $MoSe_2$.[16] The DFT semicore pseudopotential (DSSP) method and double numerical plus polarization basis set (DNP) have been

https://doi.org/10.1021/acsomega.1c01704
ACS Omega 2021, 6, 16517−16523

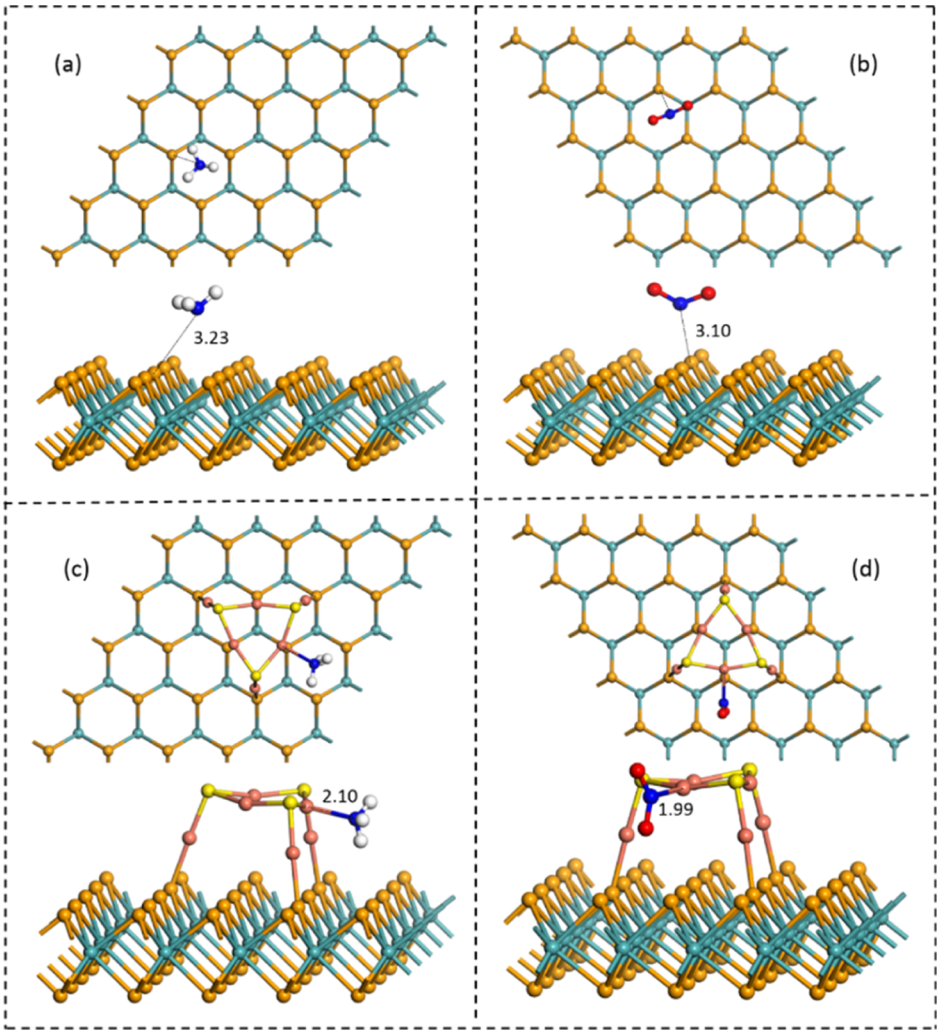

Figure 3. (a) NH_3 and (b) NO_2 adsorption on $MoSe_2$ and (c) NH_3 and (d) NO_2 adsorption on Cu_2S−$MoSe_2$.

chosen.[25] For speeding up SCF convergence, the DIIS field was set to 6, and self-consistent field tolerance was set to 10^{-6} Ha to obtain a stationary electronic structure.[26,27]

Various doping structures of Cu_2S on $MoSe_2$, and gas-sensing structures of gas molecules on $MoSe_2$/Cu_2S−$MoSe_2$ were calculated to obtain the most stable one. To analyze the adsorption properties of the target gas on Cu_2S−$MoSe_2$, adsorption energy, charge transfer, and molecular orbital analyses were considered. The adsorption energy was defined in eq 1. Where $E_{suf/gas}$ is the total energy of the adsorption system and E_{suf} and E_{gas} are the energy of the $MoSe_2$/Cu_2S−$MoSe_2$ surface and the isolated gas molecule, respectively. The charge transfer amount in the adsorption process was defined according to eq 2. Q_{iso} and Q_{ads} represent the total charge of the gas molecule before and after adsorption, respectively. If $Q > 0$, electrons transfer from the gas molecule to Cu_2S−$MoSe_2$. As defined in eq 3, the energy gap of the molecular orbit can be used to evaluate the change in conductivity of the material. Where E_{HOMO} is the energy of the highest occupied molecular orbit and E_{LUMO} represents the energy of the lowest unoccupied molecular orbit.

$$E_{ads} = E_{suf/gas} - E_{suf} - E_{gas} \quad (1)$$

$$Q_T = Q_{ads} - Q_{iso} \quad (2)$$

$$E_g = E_{LUMO} - E_{HOMO} \quad (3)$$

3. RESULTS AND DISCUSSION

3.1. Geometric Optimization of NH_3, NO_2, $MoSe_2$, and Cu_2S−$MoSe_2$. The stable structures of NH_3 and NO_2 are shown in Figure 1a,b. The NH_3 molecule shows a pyramidal structure with a N−H bond of 1.023 Å and a H−N−H angle of 106.27°. For NO_2, the bond lengths of N−O are 1.209 Å, and the V-shaped O−N−O angle is 133.36°. Figure 1c shows the stable structure of intrinsic $MoSe_2$, and the Se−Mo−Se layered structure makes it easier to adsorb and desorb gas molecules. In order to obtain the most stable doping structure of Cu_2S on the $MoSe_2$ surface, several initial approaching directions of Cu_2S to $MoSe_2$ were built and optimized, and the most stable one is shown in Figure 1d,e in side and top views. Three Cu_2S clusters form a triangular ring on $MoSe_2$, the Cu atom tends to form chemical bonds with the Se atom, and the average Cu−Se bond length is 2.26 Å. The binding energy is up to −10.775 eV, which not only indicates the adsorption process proceeds spontaneously, but also shows there is a strong interaction between the Cu_2S dopant and the $MoSe_2$ surface.

Figure 2 shows the DOS, PDOS, and energy band structure of $MoSe_2$ and Cu_2S−$MoSe_2$. In Figure 2a, after doping the

https://doi.org/10.1021/acsomega.1c01704
ACS Omega 2021, 6, 16517−16523

Cu_2S cluster, the overall DOS moved left. It is obvious that the DOS curve increases near −2 eV, which was mainly caused by the Cu-3d orbit. From the DOS curve, the orbits of Cu-3d, S-3p, Se-4p, and Mo-4d hybridize around −2.6 and 1 eV, indicating a strong interaction between Cu_2S and $MoSe_2$. From Figure 2b, it can be found that the band gap of $MoSe_2$ is 1.649 eV, signifying that it is a typical semiconductor material. After Cu_2S modification, the band gap reduces to 0.905 eV. As a result, the energy gap for electrons to jump from the valence band to the conduction band reduces, indicating a significant increase in the conductivity after Cu_2S doping.

3.2. NH_3 and NO_2 Adsorption on $MoSe_2$ and Cu_2S−$MoSe_2$ Surfaces. Figure 3 shows the most stable adsorption structures of the target gas on intrinsic $MoSe_2$ and Cu_2S−$MoSe_2$ surfaces, and the adsorption parameters of each structure are shown in Table 1. For gas adsorption on intrinsic $MoSe_2$ in Figure 3a,b, the results show that adsorption energies of NO_2 and NH_3 on the $MoSe_2$ surface were −0.17 and −0.20 eV, and the adsorption distances were 3.11, 3.23 Å, respectively. Considering the weak adsorption energy and the longer adsorption distance, the adsorption process between the target gas and $MoSe_2$ belongs to weak physisorption. In addition, according to Mulliken charge analysis, there is only 0.18 *e* electrons transferred from $MoSe_2$ to NO_2, while only 0.05 *e* electrons transfer from NH_3 to $MoSe_2$. From the analysis of adsorption energy, adsorption distance, and charge transfer, it can be concluded that the adsorption of intrinsic $MoSe_2$ is too weak to effectively adsorb NO_2 and NH_3. Therefore, intrinsic $MoSe_2$ is not an appropriate gas-sensing material for target gases.

Table 1. Adsorption Energy, Adsorption Distance, and Charge Transfer of Gas Adsorption on $MoSe_2$ and Cu_2S−$MoSe_2$

structure	E_{ads}/eV	d/Å	Q_T/e
$NH_3/MeSe_2$	−0.20	3.23	0.05
$NO_2/MoSe_2$	−0.17	3.11	−0.18
NH_3/Cu_2S−$MoSe_2$	−0.78	2.10	0.27
NO_2/Cu_2S−$MoSe_2$	−1.06	1.99	−0.19

Several initial approaching directions of target gas to the Cu_2S−$MoSe_2$ surface were built and optimized, and the most stable adsorption structures are shown in Figure 3c,d. It is obvious that both of NO_2 and NH_3 form stable chemical bonds with Cu_2S−$MoSe_2$. For NH_3, the N atom of NH_3 forms a N−Cu bond with the Cu_2S dopant. The adsorption energy of NH_3 on Cu_2S−$MoSe_2$ was −0.78 eV with an adsorption distance of 2.10 Å. Moreover, according to Mulliken charge analysis, 0.27 *e* charge transfers from NH_3 to Cu_2S−$MoSe_2$, which is distinctly more than that of the intrinsic $MoSe_2$ adsorption system. The increase in the amount of charge transfer indicates a stronger interaction. Therefore, Cu_2S-doped $MoSe_2$ greatly promotes the adsorption performance for NH_3. For NO_2, N atoms are close to the Cu atoms by forming a N−Cu bond with a bond length of 1.99 Å. The adsorption energy is −1.06 eV, and the transfer amount is −0.19 *e* electrons from Cu_2S−MoSe to NO_2. Compared with intrinsic $MoSe_2$, the adsorption distance decreases by 1.12 Å, and the absolute adsorption energy increases by 1.06 eV. The result indicates that Cu_2S−$MoSe_2$ shows a stronger adsorption performance for NO_2 than intrinsic $MoSe_2$.

3.3. Density of States Analysis of Gas Adsorption on $MoSe_2$ and Cu_2S−$MoSe_2$. The charge transfer during the adsorption process will change the redistribution of DOS, influencing the conductivity of the whole system. For further

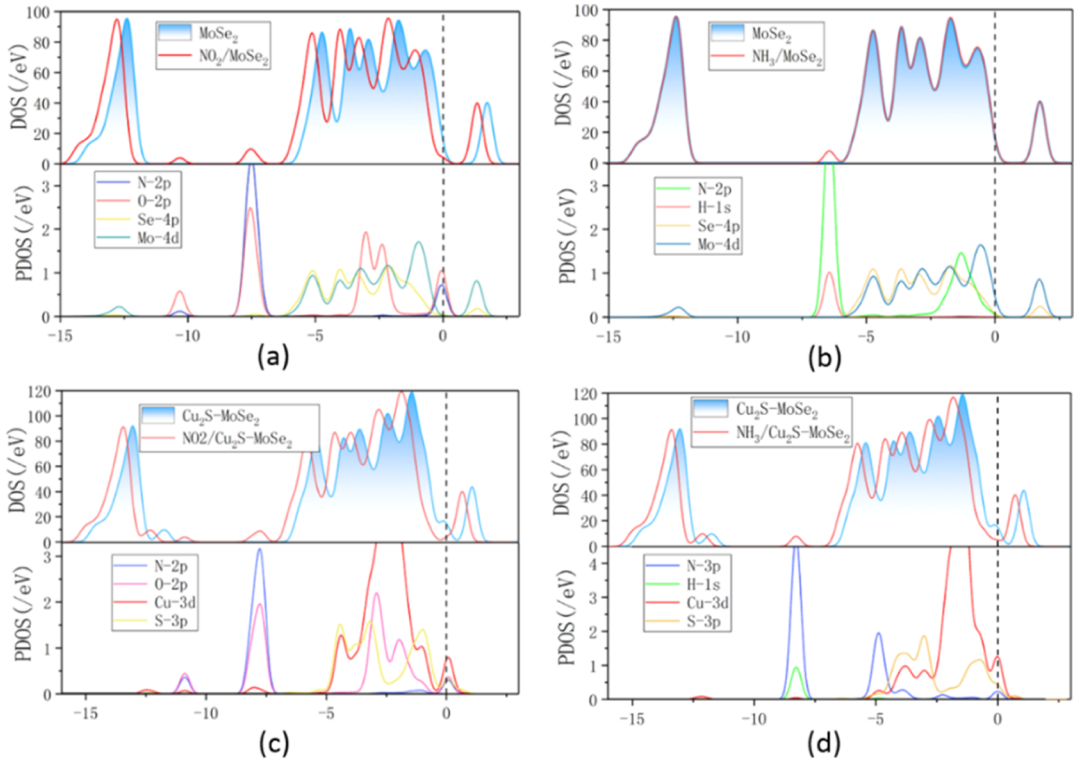

Figure 4. DOS and PDOS distribution: (a) before and after NO_2 adsorption on $MoSe_2$, (b) before and after NH_3 adsorption on $MoSe_2$, (c) before and after NO_2 adsorption on Cu_2S−$MoSe_2$, and (d) before and after NH_3 adsorption on Cu_2S−$MoSe_2$.

https://doi.org/10.1021/acsomega.1c01704
ACS Omega 2021, 6, 16517−16523

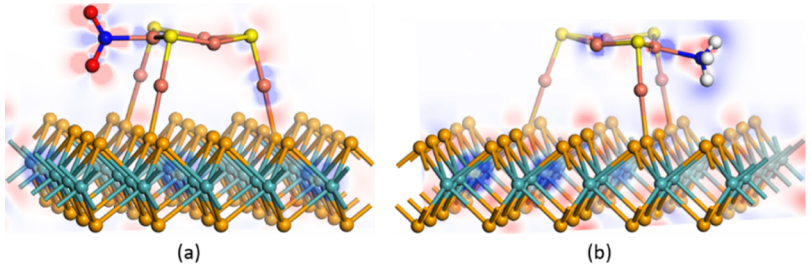

Figure 5. Charge density difference of (a) NO_2-adsorbed $Cu_2S-MoSe_2$ and (b) NH_3-adsorbed $Cu_2S-MoSe_2$.

analyzing the adsorption mechanism, DOS of intrinsic $MoSe_2$ and $Cu_2S-MoSe_2$ before and after gas adsorption were calculated, respectively, as shown in Figure 4.

From Figure 4a, it is obviously observed that DOS distribution shifts to the left as a whole after NO_2 adsorption. New peaks appearing at −10.5 and −7.5 eV were mainly attributed to by N-2p and O-2p. It indicates that NO_2 can interact with $MoSe_2$, and the result is consistent with the other research results.[28] In Figure 4b, DOS nearly not changes after NH_3 adsorption, which signifies the interaction between NH_3 and $MoSe_2$ is extremely weak. That is the reason why only 0.05 *e* charge transfer from NH_3 to $MoSe_2$. In Figure 4c, it can be found from PDOS that the overlap of Cu-3d, O-2p, and S-3p from −3 to −1.5 eV means a strong interaction between NO_2 and $Cu_2S-MoSe_2$. In addition, the orbital hybridization of Cu-3d, N-2p, and O-2p at 0 eV significantly changes the electron distribution near the Fermi energy level, leading to a change of conductivity of the adsorption system, which is of great significance to a gas sensor. Similarly, the distribution of DOS moves left after NH_3 adsorption as shown in Figure 4d. The reduction of DOS at the Fermi level indicates a decrease in the conductivity of the adsorption system. From the PDOS, it can be found that DOS variation at the Fermi energy level was mainly introduced by the orbital hybridization of Cu-3d and N-2p. This reflects that Cu and N form a coordination bond, which greatly enhances the adsorption performance.

3.4. Charge Density Difference Analysis of Gas-Adsorbed $Cu_2S-MoSe_2$. Figure 5 shows the electron density difference of NO_2/NH_3-adsorbed $Cu_2S-MoSe_2$, it intuitively displays the charge transfer after adsorption. The red and blue represent the electron reception and lost region, respectively. In Figure 5a, the whole area around NO_2 is red, indicating that NO_2 has obtained electrons from $Cu_2S-MoSe_2$. The charge distribution on N−Cu bonds is very dense, which means that a strong interaction occurs between Cu and N atoms. The results show the Cu atom plays an important role in NO_2adsorption. In Figure 5b, the N atom of NH_3 gains electrons, but all three H atoms lose electrons. The amount of charge lost is more than the gained, so the surrounding of NH_3 is shown in blue. A large number of electron transfer indicates that $Cu_2S-MoSe_2$ has a good adsorption effect on NH_3.

3.5. Molecular Orbital Analysis of NO_2 and NH_3 Adsorption on $Cu_2S-MoSe_2$. The conductivity of materials can be evaluated by the energy gap, and a smaller energy gap represents a higher conductivity.[29] The HOMO−LUMO of $Cu_2S-MoSe_2$ and gas-adsorbed $Cu_2S-MoSe_2$ was calculated based on the molecular orbital theory as shown in Figure 6. For $Cu_2S-MoSe_2$, the HOMO mainly locates on Cu_2S and the LUMO locates mainly on Mo atoms. The energy gap of 0.95 eV indicates that it is a typical semiconductor material. After NH_3 adsorption, the HOMO distribution on the Cu_2S doping

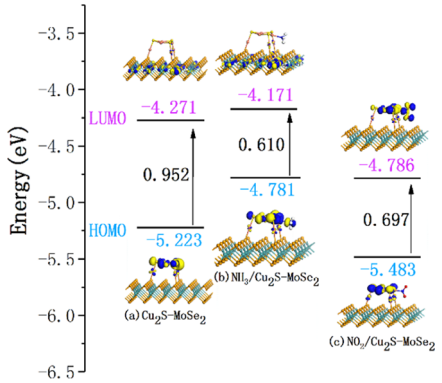

Figure 6. Molecular orbit analysis of NO_2 and NH_3 adsorbed on $Cu_2S-MoSe_2$.

area slightly increases, and it extends to the adsorbed NH_3 molecule. The energy gap decreases to 0.610 eV, leading to an increase of the conductivity of the adsorption system. For NO_2 adsorption, the LUMO distribution dramatically increases compared with those of intrinsic $Cu_2S-MoSe_2$ and $NH_3/Cu_2S-MoSe_2$, resulting in a great decrease of the energy level of LUMO. As a result, the energy gap is only 0.697 eV. In summary, adsorption of both NH_3 and NO_2 leads to an increase of conductivity of the adsorption systems.

3.6. Recovery Time. The recovery time (τ) is an important parameter in assessing the performance of a gas-sensing material.[30] Theoretically, the recovery time can be evaluated according to eq 4

$$\tau = \nu^{-1} \exp(-E_{ads}/KT) \quad (4)$$

where K is the Boltzmann constant (8.62×10^{-5} eV/K), T is the temperature, ν indicates the attempted frequency (10^{12} s^{-1}). Figure 7 shows the recovery time for NH_3 and NO_2 adsorption on $Cu_2S-MoSe_2$ at different temperatures. It can be seen from the curve that the recovery time decreases with the increase of the ambient temperature. An appropriate recovery time represents the reversibility of a gas sensor can be better. However, too short recovery time also means that the adsorption ability is too weak to realize the gas-sensing response, which is not conducive to gas detection. At room temperature (298 K), the recovery time for NH_3 adsorption on $Cu_2S-MoSe_2$ is 15.39 s. It is obvious that $Cu_2S-MoSe_2$ is extremely suitable as an NH_3 sensor at room temperature. For NO_2, the recovery time drops to 22.45 s when the temperature increases to 400 K. In actual situation, the optimal heating temperature of $Cu_2S-MoSe_2$ ranges from ambient temperature to 400 K.

https://doi.org/10.1021/acsomega.1c01704
ACS Omega 2021, 6, 16517−16523

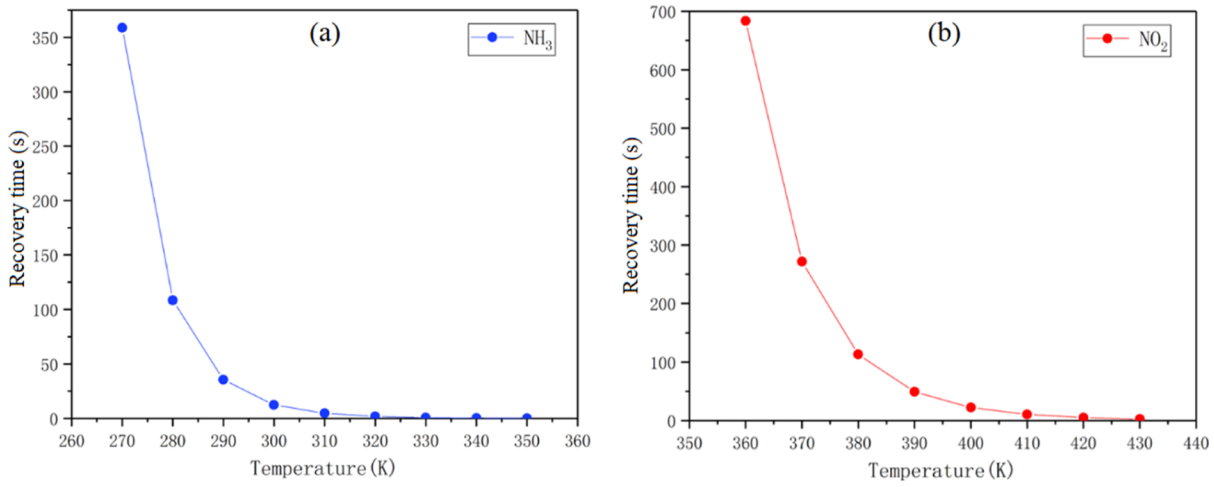

Figure 7. Recovery time for (a) NH_3 and (b) NO_2 adsorption on Cu_2S−$MoSe_2$ at different temperatures.

4. CONCLUSIONS

In this work, the adsorption and gas-sensing properties of Cu_2S−$MoSe_2$ to NO_2 and NH_3 gases were investigated by DFT calculations. The adsorption structures, density of states, molecular orbit, and recovery time were calculated to analyze the gas-sensing mechanism of gas-adsorbed Cu_2S−$MoSe_2$. The Cu_2S cluster provides active adsorption sites on the $MoSe_2$ surface, and also increases the conductivity of the doping system. Due to chemisorption, Cu_2S−$MoSe_2$ shows higher absolute adsorption energy and a shorter adsorption distance than intrinsic $MoSe_2$ upon NO_2 and NH_3 adsorption, indicating Cu_2S cluster modification effectively improves the adsorption performance of intrinsic $MoSe_2$. DOS analysis shows Cu-3d and S-3p of Cu_2S hybridize with the atoms of NO_2 and NH_3. Charge density difference analysis reveals the losing and gaining process upon NO_2 and NH_3 adsorption, respectively. As a result, conductivity of the adsorption system enhances after NH_3/NO_2 adsorption on Cu_2S−$MoSe_2$. The recovery time shows that Cu_2S−$MoSe_2$ can be a good gas-sensing material for NH_3 detection at room temperature (298 K), while NO_2 detection needs a high temperature of 400 K. Based on the theoretical calculation results, the Cu_2S−$MoSe_2$-based gas sensor can be used to detect toxic gases with high efficiency.

AUTHOR INFORMATION

Corresponding Author

Yingang Gui − *Faculty of Quality Management and Inspection & Quarantine, Yibin University, Yibin 644000, China; College of Engineering and Technology, Southwest University, Chongqing 400715, China;* orcid.org/0000-0003-1424-7082; Email: yinganggui@swu.edu.cn

Authors

Shengyan Zhu − *Faculty of Quality Management and Inspection & Quarantine, Yibin University, Yibin 644000, China*

Xianping Chen − *College of Optoelectronic Engineering and Key Laboratory of Optoelectronic Technology & Systems Education Ministry of China, Chongqing University, Chongqing 400044, China;* orcid.org/0000-0002-6332-0955

Complete contact information is available at: https://pubs.acs.org/10.1021/acsomega.1c01704

Notes

The authors declare no competing financial interest.

ACKNOWLEDGMENTS

This work is supported by the National Natural Science Foundation of China (grant no. 51907165), Chongqing Research Program of Basic Research and Frontier Technology (grant no. cstc2018jcyjAX0068), and the Fundamental Research Funds for the Central Universities (grant no. XDJK2020B024).

REFERENCES

(1) Samaddar, P.; Son, Y.-S.; Tsang, D. C. W.; Kim, K.-H.; Kumar, S. Progress in graphene-based materials as superior media for sensing, sorption, and separation of gaseous pollutants. *Coord. Chem. Rev.* **2018**, *368*, 93−114.

(2) Huang, T.; Lou, Z.; Chen, S.; Li, R.; Jiang, K.; Chen, D.; Shen, G. Fabrication of rigid and flexible $SrGe_4O_9$ nanotube-based sensors for room-temperature ammonia detection. *Nano Res.* **2017**, *11*, 431−439.

(3) Salih, E.; Ayesh, A. I. Enhancing the sensing performance of zigzag graphene nanoribbon to detect NO, NO_2, and NH_3 gases. *Sensors* **2020**, *20*, 3932.

(4) Li, H.-Y.; Lee, C.-S.; Kim, D. H.; Lee, J.-H. Flexible room-temperature NH_3 sensor for ultrasensitive, selective, and humidity-independent gas detection. *ACS Appl. Mater. Interfaces* **2018**, *10*, 27858−27867.

(5) Lee, K.; Shim, Y.-S.; Song, Y.; Han, S.; Lee, Y.-S.; Kang, C.-Y. Highly sensitive sensors based on metal-oxide nanocolumns for fire detection. *Sensors* **2017**, *17*, 303.

(6) Zhang, D.; Yang, Z.; Li, P.; Pang, M.; Xue, Q. Flexible self-powered high-performance ammonia sensor based on Au-decorated $MoSe_2$ nanoflowers driven by single layer MoS_2-flake piezoelectric nanogenerator. *Nano Energy* **2019**, *65*, 103974.

(7) Zhang, D.; Jiang, C.; Li, P.; Sun, Y. e. Layer-by-layer self-assembly of Co_3O_4 nanorod-decorated MoS_2 nanosheet-based nanocomposite toward high-performance ammonia detection. *ACS Appl. Mater. Interfaces* **2017**, *9*, 6462−6471.

(8) Chen, X.; Chen, X.; Han, Y.; Su, C.; Zeng, M.; Hu, N.; Su, Y.; Zhou, Z.; Wei, H.; Yang, Z. Two-dimensional $MoSe_2$ nanosheets via liquid-phase exfoliation for high-performance room temperature NO_2 gas sensors. *Nanotechnology* **2019**, *30*, 445503.

(9) Yang, A.; Wang, D.; Lan, T.; Chu, J.; Li, W.; Pan, J.; Liu, Z.; Wang, X.; Rong, M. Single ultrathin WO_3 nanowire as a superior gas

sensor for SO_2 and H_2S:Selective adsorption and distinct I-V response. *Mater. Chem. Phys.* **2020**, *240*, 122165.
(10) Wang, D.; Yang, A.; Lan, T.; Fan, C.; Pan, J.; Liu, Z.; Chu, J.; Yuan, H.; Wang, X.; Rong, M.; Koratkar, N. Tellurene based chemical sensor. *J. Mater. Chem. A* **2019**, *7*, 26326−26333.
(11) Late, D. J.; Doneux, T.; Bougouma, M. Single-layer $MoSe_2$ based NH_3 gas sensor. *Appl. Phys. Lett.* **2014**, *105*, 233103.
(12) Chu, J.; Li, W.; Yang, X.; Wu, Y.; Wang, D.; Yang, A.; Yuan, H.; Wang, X.; Li, Y.; Rong, M. Identification of gas mixtures via sensor array combining with neural networks. *Sens. Actuators, B* **2021**, *329*, 129090.
(13) Ma, S.; Su, L.; Jin, L.; Su, J.; Jin, Y. A first-principles insight into Pd-doped $MoSe_2$ monolayer: A toxic gas scavenger. *Phys. Lett. A* **2019**, *383*, 125868.
(14) Rathi, K.; Pal, K. Fabrication of $MoSe_2$−graphene hybrid nanoflakes for toxic gas sensor with tunable sensitivity. *Adv. Mater. Interfaces* **2020**, *7*, 2000140.
(15) Ai, W.; Kou, L.; Hu, X.; Wang, Y.; Krasheninnikov, A. V.; Sun, L.; Shen, X. Enhanced sensitivity of $MoSe_2$ monolayer for gas adsorption induced by electric field. *J. Phys.: Condens. Matter* **2019**, *31*, 445301.
(16) Qian, H.; Deng, J.; Xie, Z.; Pan, Z.; Zhang, J.; Zhou, H. Adsorption and gas sensing properties of the Pt3-$MoSe_2$ Monolayer to SOF_2 and SO_2F_2. *ACS Omega* **2020**, *5*, 7722−7728.
(17) Gui, Y.; Shi, J.; Xu, L.; Ran, L.; Chen, X. Au_n (n=1−4) cluster doped $MoSe_2$ nanosheet as a promising gas-sensing material for C_2H_4 gas in oil-immersed transformer. *Appl. Surf. Sci.* **2020**, *541*, 148356.
(18) Xu, L.; Liu, Y.; Gui, Y.; Zhang, Q.; Chen, X. Adsorption property of CO, NO, and NO_2 gas molecules on Co3-$MoSe_2$ monolayer. *Sens. Actuators, A* **2021**, *319*, 112547.
(19) Hassan, M. S.; Bera, S.; Gupta, D.; Ray, S. K.; Sapra, S. $MoSe_2$-Cu_2S vertical p-n nanoheterostructures for high-performance photodetectors. *ACS Appl. Mater. Interfaces* **2019**, *11*, 4074−4083.
(20) Gui, Y.; Shi, J.; Yang, P.; Li, T.; Tang, C.; Xu, L. Platinum modified MoS_2 monolayer for adsorption and gas sensing of SF_6 decomposition products: a DFT study. *High Voltage* **2020**, *5*, 454−462.
(21) Zhang, X.; Yu, L.; Wu, X.; Hu, W. Experimental sensing and density functional theory study of H_2S and SOF_2 adsorption on Au-modified graphene. *Adv. Sci.* **2015**, *2*, 1500101.
(22) He, X.; Gui, Y.; Xie, J.; Liu, X.; Wang, Q.; Tang, C. A DFT study of dissolved gas (C_2H_2, H_2, CH_4) detection in oil on CuO-modified BNNT. *Appl. Surf. Sci.* **2020**, *500*, 144030.
(23) Gui, Y.; Peng, X.; Liu, K.; Ding, Z. Adsorption of C_2H_2, CH_4 and CO on Mn-doped graphene: Atomic, electronic, and gas-sensing properties. *Physica E* **2020**, *119*, 113959.
(24) Cui, H.; Chen, D.; Zhang, Y.; Zhang, X. Dissolved gas analysis in transformer oil using Pd catalyst decorated $MoSe_2$ monolayer: A first-principles theory. *Sustainable Mater. Technol.* **2019**, *20*, No. e00094.
(25) Cui, H.; Liu, T.; Zhang, Y.; Zhang, X. Ru-InN monolayer as a gas scavenger to guard the operation status of SF_6 insulation devices: A first-principles theory. *IEEE Sens. J.* **2019**, *19*, 5249−5255.
(26) Li, P.; Hong, Q.; Wu, T.; Cui, H. SOF_2 sensing by Rh-doped PtS_2 monolayer for early diagnosis of partial discharge in the SF_6 insulation device. *Mol. Phys.* **2021**, *119*, 113276.
(27) Cui, H.; Zhang, G.; Zhang, X.; Tang, J. Rh-doped $MoSe_2$ as a toxic gas scavenger: a first-principles study. *Nanoscale Adv.* **2019**, *1*, 772−780.
(28) Liu, Y.; Shi, T.; Si, Q.; Liu, T. Adsorption and sensing performances of transition metal (Pd, Pt, Ag and Au) doped $MoTe_2$ monolayer upon NO_2: A DFT study. *Phys. Lett. A* **2021**, *391*, 127117.
(29) Yin, X.; Li, Y.; Zhang, Y.; Li, P.; Zhao, J. Theoretical analysis of geometry-correlated conductivity of molecular wire. *Chem. Phys. Lett.* **2006**, *422*, 111−116.
(30) Liu, H.; Xu, L.; Gui, Y.; Ran, L.; Chen, X. Adsorption properties of Ag_2O−$MoSe_2$ towards SF_6 decomposed products. *Vacuum* **2021**, *189*, 110248.

https://doi.org/10.1021/acsomega.1c01704
ACS Omega 2021, 6, 16517−16523